Stucki, P., A. Baumann, and D. Bucher (2017) The 1978 Heavy Precipitation and Flood Event in Switzerland. In: Brönnimann, S. (Ed.) *Historical Weather Extremes in Reanalyses.* Geographica Bernensia G92, p. 69-80, DOI: 10.4480/GB2017.G92.06.

The 1978 Heavy Precipitation and Flood Event in Switzerland

Peter Stucki*, Aline Baumann, and Dominique Bucher

Oeschger Centre for Climate Change Research and Institute of Geography, University of Bern, Switzerland

Abstract

On 7-8 August 1978, severe floods and debris flows, induced by heavy precipitation with embedded thunderstorms, occurred on both north and south sides of the Swiss Alps. On the north side, northeastern Switzerland and the Rhine was affected, on the south side, mainly an area near Lago Maggiore. The associated synoptic weather patterns and dynamics are analysed using the Twentieth Century Reanalysis (20CRv2c) dataset, and in addition using the NCEP/NCAR, ERA-20C and CERA-20C reanalyses. Responsible for the heavy precipitation was an upglide process of warm moist air from the south over and across the Alps. These dynamics were related to a 'Vb-type' lee surface low, a quasi-stationary front over the Alps, and marked upper-level ascent of air downstream of a 'digging trough'. The atmospheric features are well represented in the 20CRv2c dataset, with restrictions regarding the orographic modulation of the moisture flow and intensity of precipitation, for instance. Differences to the three other reanalyses products, two with finer resolution, are overall small.

1. Introduction

The Central Alps form a natural barrier for large-scale moisture transport. Large elevation differences, steep terrain and often concave topography force advected moist air to rise and condensate (Frei and Schär, 1998). In Switzerland, two Alpine regions are particularly exposed to heavy precipitation events and subsequent floods: the pre-alpine ranges in northern Switzerland, and the south side of the Alps.

Here, we investigate a severe flood event induced by heavy-precipitation on both sides of the Alps. On 7 August 1978, intense and prolonged precipitation in large areas of the Rhine

* Corresponding author: Peter Stucki, University of Bern, Institute of Geography, Hallerstr. 12, CH-3012 Bern, Switzerland. E-mail: peter.stucki@giub.unibe.ch

catchment led to a flood event on the north side of the Alps that was labelled ‘centennial’ and ‘unpredictable’ at the time (Courvoisier et al., 1979; Scherrer et al., 2006; Aebischer, 1997). Around noon on 8 August 1978, the discharge of the Rhine in Basel reached a maximum of 4150 $m^3 s^{-1}$, equal to a discharge of a 100-year event at that time (Scherrer et al., 2006). Losses of more than 30 million CHF accrued along the river Thur alone (Röthlisberger, 1991; Fig. 1, top).

On the south side of the Alps, a large number of floods, debris flows and log jamming led to widespread erosion and devastations of settlements, roads and other infrastructure (Röthlisberger, 1991). For instance, log jamming on a high-mountain reservoir caused an instant overflow of 2000 $m^3 s^{-1}$ at the dam (Hauenstein, 2009; Fig. 1, bottom).

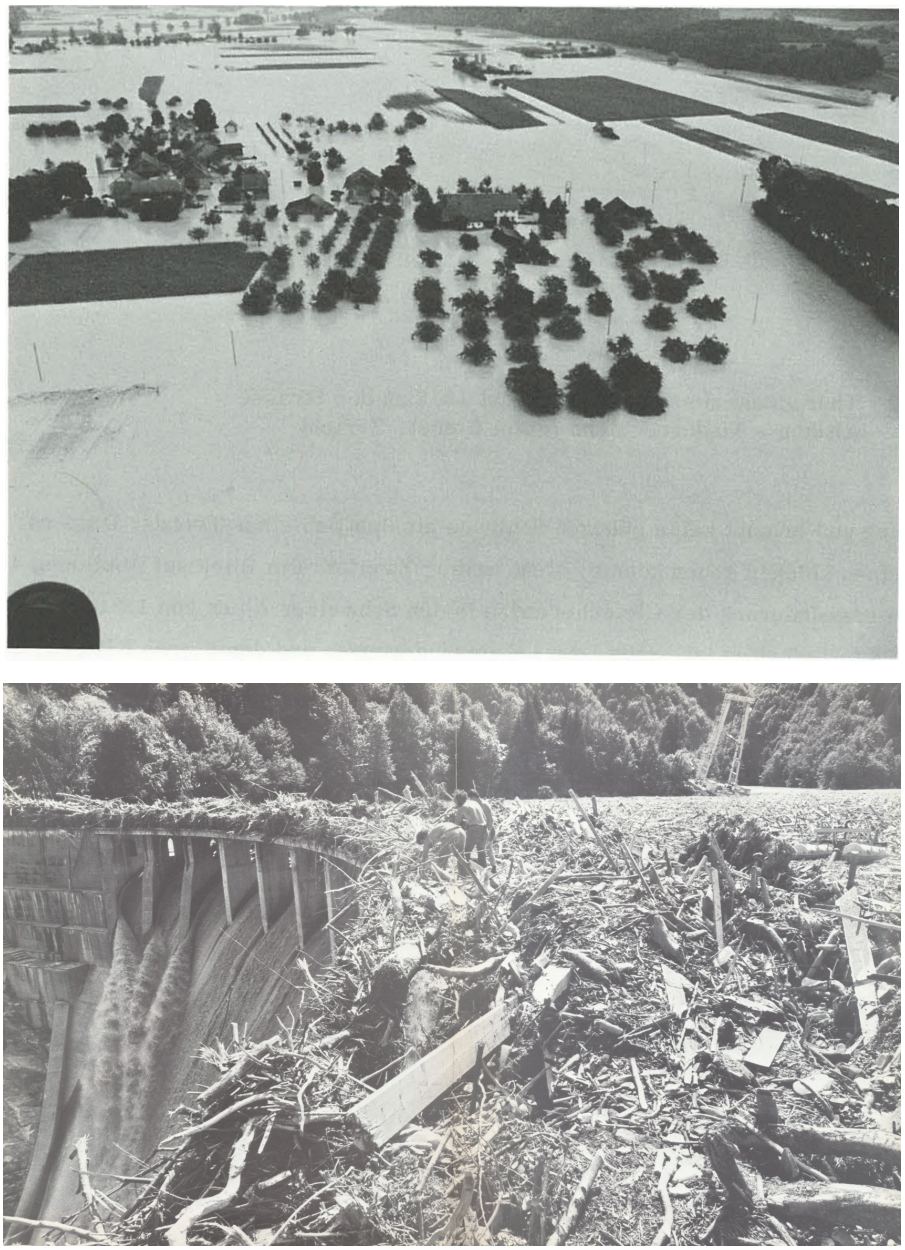

Figure 1. (top) Flooding on 7 August 1978 along the Thur river (from VAW, 1978, photo by Comet, Zürich). (bottom) Log jamming on the Palagnedra reservoir (from “Giornale del Popolo”, see Heitmann and Zanetti, 1978).

A peak discharge of 4500 $m^3 s^{-1}$ was estimated for the Maggia, a major contributary river to Lago Maggiore and known to react very rapidly and strongly to heavy precipitation (Conca, 1979; FOEN, 2017). Luckily, a potentially catastrophic dam breakage could be prevented. The Lago Maggiore water level was relatively low before the event such that the increase of 2.11 m from 6 to 9 August 1978 did not cause an extreme flood. Nevertheless, the total damage in the region accrued to approx. 100 million CHF.

Key meteorological ingredients for such flood-producing heavy precipitation are conditional instability of atmospheric layers, enabling synoptic-scale ascent of air, meso-scale forced ascent by a mountain barrier such as the Alps, and sufficiently available moisture in the atmosphere (Doswell et al., 1996). Important are also the amplitude of the (low-level, convergent) moisture flux and the advection relative to the topography (Piaget et al., 2011; Froidevaux et al., 2013).

In the specific case of the 7-8 August 1978 event, the hydrological and meteorological dynamics of the high-precipitation and subsequent flood event were well documented, *e.g.,* by Courvoisier et al. (1979). They identified a mid-tropospheric cold-air trough, reaching south to and consolidating over the Iberian Penninsula prior to the event. Then, its southern (around 45° N) part propagated from longitude 10° W to around 5–8° E, and led to a very strong meridional air flow over the western Mediterranean on 7 August 1978. A 'Vb-type lee surface cyclone' (cf. van Bebber, 1891) formed south of the Alps. The associated surface cold front reached the north side of the Alps in the course of the day, while ahead of the cold front, there was sustained advection of moist and warm air from the Mediterranean Sea towards the south side of the Alps. As a consequence, the moist-warm, unstable air mass moved over the cold air in the northern Alps and over western Switzerland. The key components for the heavy precipitation event were found in the combination of synoptic mid-tropospheric ascent of air with very high absolute specific humidity, maximum diurnal heating, and southerly advection of very moist tropical air impinging on the Alpine topography. The quasi-stationarity of the frontal system over the Alpine divide lasted over several hours, with NE-propagating massive thunderstorm systems across the Alps (no 'Staulage' due to instability over the Alps), leading to large-scale and heavy precipitation with embedded thunderstorms on both sides of the Alpine divide. The most intense phase of heavy precipitation occurred from late afternoon to around midnight on 7 August 1978.

In this article, we aim at reproducing relevant meteorological features of this heavy precipitation event. For this, we use four atmospheric reanalysis products. In Section 2, we introduce the used global reanalyses and the local precipitation observations. In Section 3, we present the analyses of the synoptic-scale meteorological patterns and the local precipitation distribution. In Section 4, we compare the quality of the reproduced synoptic features among the reanalysis products and with existent knowledge, *e.g.,* from contemporary meteorological reports such as Courvoisier et al. (1979). While the meso-scale dynamics cannot be analysed explicitly, the local precipitation field and further documentary information can be used as a reference when discussing the results. In Section 5, we provide a short summary and conclusions.

2. Data and Methods

The synoptic analyses in this study are conducted using four atmospheric reanalysis products. The first and main dataset used is the Twentieth Century Reanalysis Version 2c (20CRv2c; Compo et al., 2011). It is a global, six-hourly (three-hourly for precipitation), four-dimensional dataset reaching back to 1851. 20CRv2c is based on the assimilation of surface pressure information from the International Surface Pressure Databank (ISPD) project (Cram et al., 2015; see Fig. 2 for the spatial distribution of the pressure information and the orography in 20CRv2c). Monthly sea surface temperature and sea ice concentrations serve as boundary conditions. The spatial resolution is 2° x 2°, which corresponds to approximately 200 x 200 km over Switzerland, and the dataset contains 31 levels in the vertical axis. The assimilation has 56 ensemble members; the ensemble mean is used here. The second dataset is the ERA-20C reanalysis (Poli et al., 2016). It spans the period 1900 to 2010, has a finer horizontal grid (approximately 125 km), more levels in the vertical (37) and a temporal resolution of three hours. In addition to surface pressure, also marine wind information is assimilated. The third reanalysis is CERA-20C (Laloyaux et al., 2016), a coupled climate reanalyses of the 20th century ranging from 1901-2010. It has a grid spacing of approx. 125 km, 91 levels in the vertical, and a temporal resolution of 3 hours. The assimilation includes surface pressure and marine wind observations as well as ocean temperature and salinity profiles. Here, we use the mean of 10 ensemble members. The fourth global dataset used is the NCEP/NCAR reanalysis (Kalnay et al., 1996). It spans the period from 1948 to the present, horizontal grid spacing is 2.5° x 2.5°, there are 17 levels in the vertical, and the temporal resolution is six hours. It assimilates aircraft and satellite information, among others. An overview of all data sets used in this book is given in the introductory paper (Brönnimann, 2017).

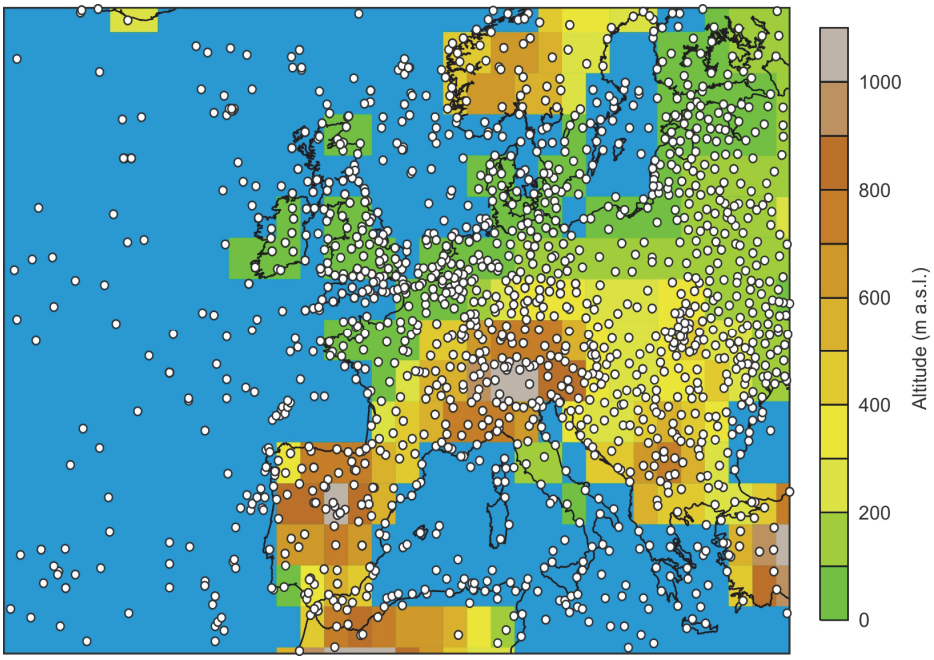

Figure 2. Location of surface pressure information from the ISPD project (filled circles) assimilated in 20CRv2c. Shown are all locations delivering pressure information between 7 August 1987 6:00 UTC and 12:00 UTC. Orography (terrain elevation in m a.s.l.) and grid spacing (boxes) in 20CRv2c are shown in colour shade.

Precipitation measurements at 507 stations come from the Swiss Federal Office of Meteorology and Climatology MeteoSwiss. The very dense network of precipitation stations in Switzerland provides very good information to describe the temporal evolution and spatial distribution of the precipitation at local scales.

Atmospheric dynamics at upper-levels are assessed using geopotential heights and vertical flow (the omega variable ω) at 500 hPa. Frontal structures (by means of Θ_e), and air flow are analysed at the 850 hPa level, and proneness to thunderstorms using the total totals index TT = (T850 - T500) + (Td850 - T500) or TT = T850 + Td850 - (2 x T500), where T850, T500, and T850 are (dew point) air temperature values at the respective hPa levels. Analysed surface variables are mean sea-level pressure, precipitation rates (calculated as mm/24 h), and precipitable water (calculated as a mono-level or entire-troposphere variable). The analyses are done visually by looking at spatial and temporal patterns, and by assessing the available quantitative information.

3. Results

3.1 Distribution of precipitation

After a first episode of heavy precipitation on 1 August 1978 south of the Alps (with precipitation amounts of >100 mm/24 h), no to little precipitation was observed in Switzerland between 2 and 5 August 1978. On 6 August 1978, intense precipitation (up to approx. 80 mm/24 h) fell in two bands stretching along the northwestern parts of Switzerland and from the south side of the Alps to southeastern Switzerland. On 7 August 1978, the precipitation peaked on both sides of the Alps (Fig. 3).

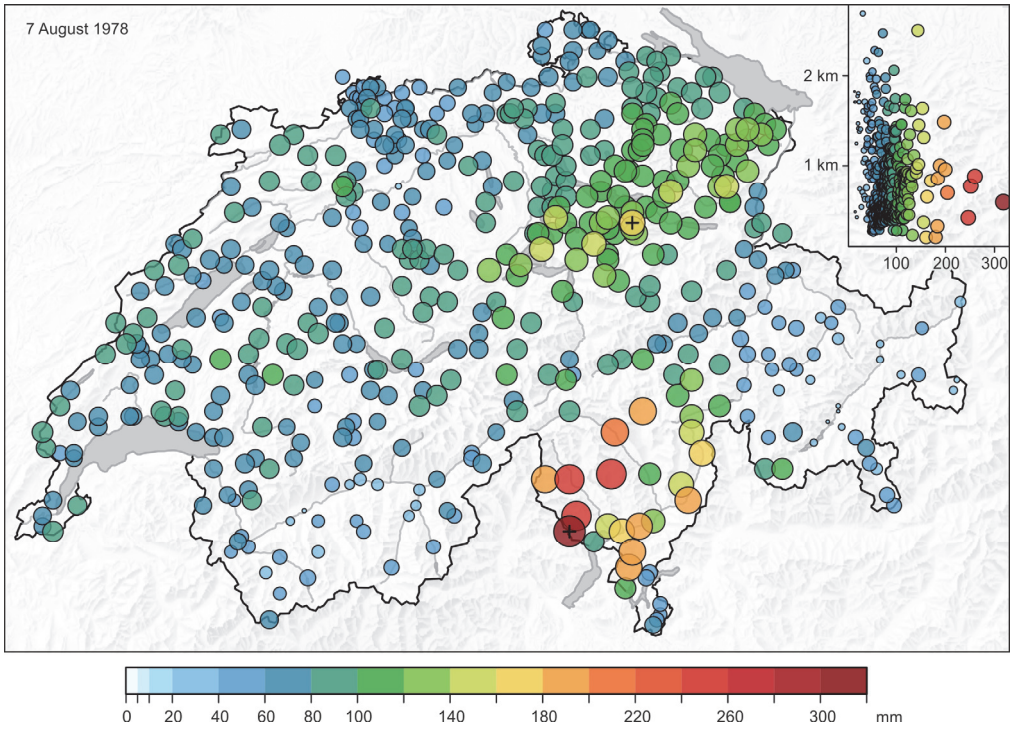

Figure 3. Measured precipitation amounts (mm/24 h) at 507 stations in Switzerland between 7 August 1978 05:40 local time and 8 August 1978 05:40 local time. Crosses mark the largest precipitation amounts north and south of the Alps. The inset shows precipitation amounts w.r.t. station elevation.

The measured daily precipitation sums were very heterogeneous in the main center of activity, located south of the Alps in the Canton of Ticino. Here, amounts of >150 mm/24 h were observed at many stations, with the largest amount of 318 mm/24 h measured at Camedo. A second center was located over the northeastern Alps of Switzerland. Intensities were markedly lower in this region (maximum of 163 mm/24 h at Rempen), and precipitation intensities were less heterogeneous. Again, precipitation intensities were independent of elevation. Only scattered showers were observed on 8 August 1978 (not shown).

3.2 Meteorological features in 20CRv2c

The analyses of meteorological features in 20CRv2c focus on the synoptic scale during the initial and core phase of the heavy precipitation event, *i.e.,* on 7 August 1978 12 and 18 UTC. In 20CRv2c, the axis of a mid-tropospheric (500 hPa level) trough extends from northern France to Spain (Fig. 4, upper left panel) on 7 August 1978 12:00 UTC. Downstream, Switzerland is located in an area of increased vertical flow (ω of -1.1 Pa s^{-1}). Here, the isotherms cross the isohypses in a more meridional orientation, which points to baroclinicity and substantial warm air advection from the south.

The associated frontal structures become apparent at the 850 hPa level, with high (low) values of Θ_e to the southeast (northwest) of Switzerland (Fig. 4, middle left panel). The moist-warm air to the south is advected towards the Alps in a very strong air flow, while winds on the north side of the Alps remain north-westerly. In addition, the Alps are located in an area with increased values of the total totals index (>45 °C), indicating high likeliness of thunderstorm activity.

At the surface, a marked low-pressure system has moved from the Balearic Sea south of Spain towards the Ligurian Sea south of the Alpine bow (Fig. 4, lower left panel; see also Fig. 5). On its northern flank, air with high precipitable water approaches the Alps. The 20CRv2c data indicate precipitation rates of up to 80 mm/24 h on 7 August 1978 06:00 UTC, and up to 100 mm/24 h over the Swiss Alps on 7 August 1978 12:00 UTC (Fig. 4, bottom panels).

Six hours later, on 7 August 1978 18:00 UTC, the mid-tropospheric trough has slightly amplified, deepened and propagated to the southeast (Fig. 4, top right panel). This pattern is often described as a 'digging trough' (*e.g.,* Lackmann, 2012; see also Fig. 6, right panel, for the situation on 8 August 1978 00:00 UTC). The areas of increased mid-tropospheric uplift and baroclinicity have slightly shifted eastward. Still, the frontal structures at 850 hPa remain almost stationary over the Alps with only a slight shift of high Θ_e values and backing wind towards the southeast, and a persistently high total totals index (Fig. 4, middle right panel). The surface low has also deepened and reaches more into the eastern Alps over Austria, the same as the area of most intense precipitation (Fig. 4, lower right panel).

4. Discussion

4.1 Surface variables in four reanalyses products

In this section, surface (or mono-level) variables in 20CRv2c are compared to NCEP/NCAR, ERA-20C and CERA-20C data. Concretely, the situation on 7 August 1978 12:00 UTC is analysed using plots of mean sea-level pressure, 10-m wind and precipitable water; the latter

is preferred over precipitation rates due to uncertainty regarding the covered timeframes. Overall, the patterns are largely similar among the reanalyses. All reanalyses feature the Azores High (*e.g.*, the 1026 hPa isobar) at very similar locations, and all of them show a large

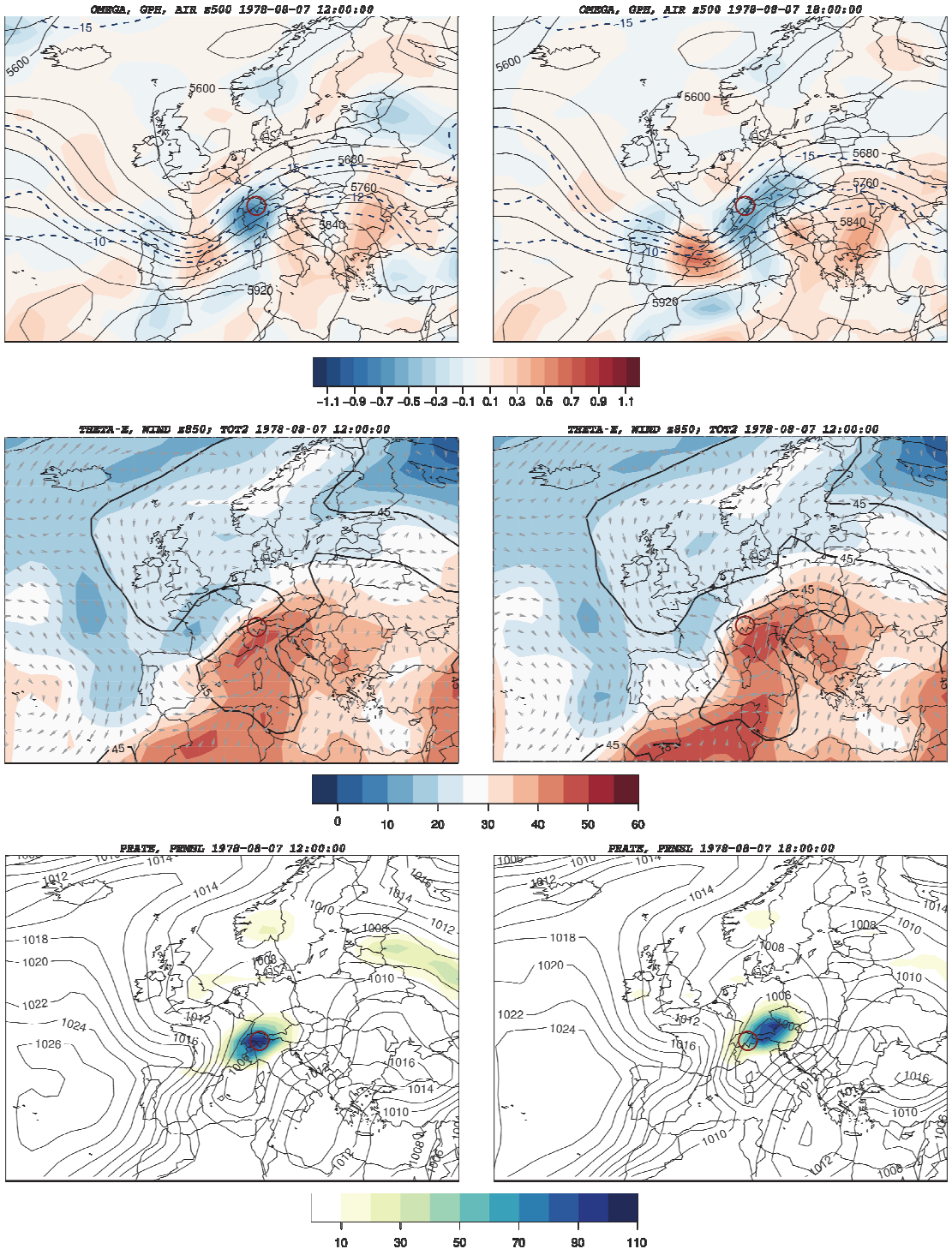

Figure 4. Geopotential height (countours; gpm), omega ω (shade; Pa s^{-1}) and air temperature at the 500 hPa level (blue dashed line; °C; top panels); Θ_e (shade; °C), total totals index (°C, black solid line), and wind (vectors) at the 850 hPa level (middle panels); mean sea-level pressure (hPa) and 3-hourly precipitation rate (shade; mm/24 h; bottom panels) for 7 August 1978 12:00 UTC (left panels) and 18:00 UTC (right panels, from 20CRv2c).

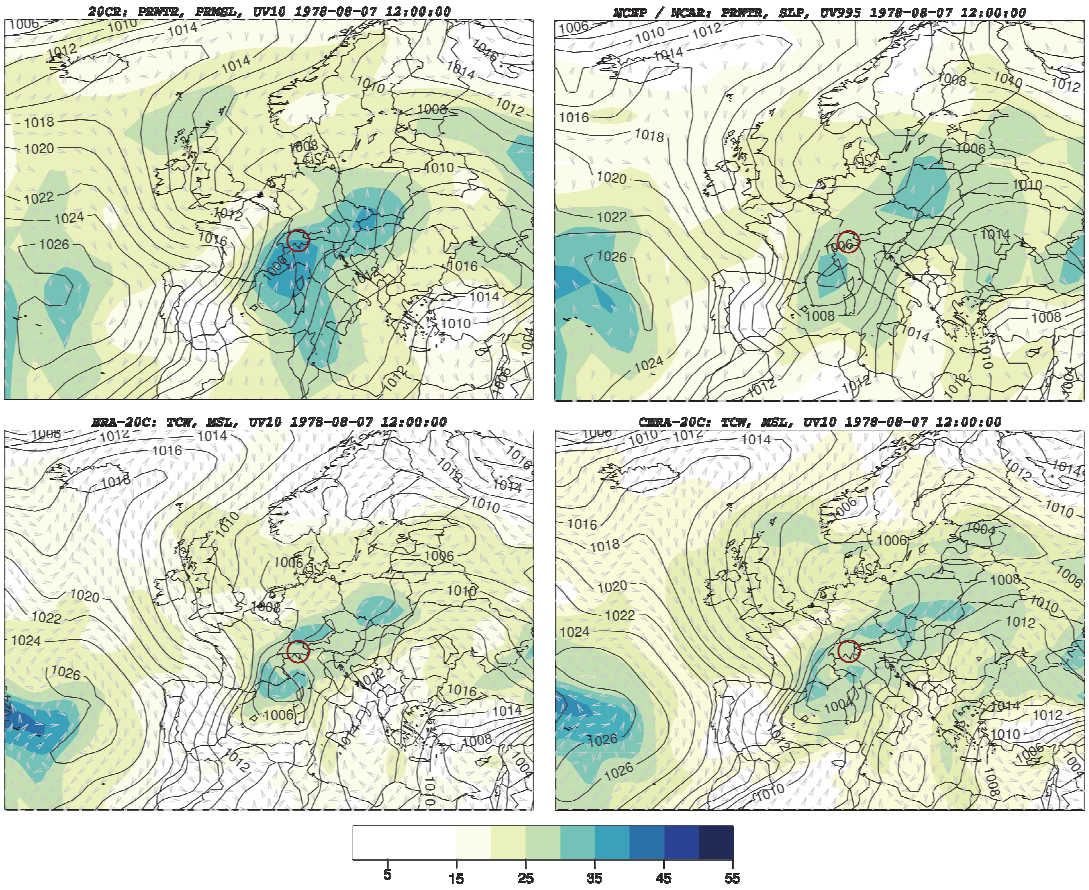

Figure 5. Surface analyses for 7 August 1978 12:00 UTC from 20CRv2c (top left panel), NCEP/NCAR (top right panel), ERA-20C (bottom left panel), and CERA-20C (bottom right panel). Shown are precipitable water (top panels) and total cloud water (bottom panels; shade in kg m^{-2} s^{-1}), mean sea-level pressure (contours) and wind at 10 m (at the 0.995 sigma level for NCEP/NCAR; vectors; every second vector is shown for ERA-20C and CERA-20C).

pressure gradient across southern France, an adjacent, marked low-pressure system over the Ligurian Sea, and increasing pressure over the eastern Mediterranean. Patches of increased precipitable water are found in the area of the Ligurian surface low and stretching towards Eastern Europe while following the Alpine bow. The central Alps are located between northwesterly flow farther north and southeasterly flow farther south.

Differences of 20CRv2c with respect to the other three reanalyses products can be found when looking at more details. For instance, 20CRv2c shows a larger area and higher amounts of precipitable water over the southern part of the Alpine bow (up to approx. 40 kg m^{-2} s^{-1} versus approx. 35 kg m^{-2} s^{-1} in NCEP/NCAR, ERA-20C and CERA-20C). The Ligurian low is a little less deep in 20CRv2c (<1006 hPa in the core area versus <1004 hPa in NCEP/NCAR, ERA-20C and CERA-20C). Over Switzerland, the ERA-20C and CERA-20C reanalyses show an area of calm winds which is missing in 20CRv2c and NCEP/NCAR. This is due to the coarser horizontal grid spacing of the latter two. Overall, 20CRv2c is able to reproduce the large-scale features very well, with slight compromises in intensities and spatial delineation compared to the finer resolved reanalyses. The differences in precipitable water are harder to assess as they might also stem from differing calculations, *e.g.,* between 20CRv2c and NCEP/NCAR on one side and the two other products on the other side. From visual analyses, CERA-20C appears to produce somewhat finer spatial structures in the meteorological features than ERA-20C, although differences are overall small.

4.2. Upper-air variables in 20CRv2c and an operational weather map

A comparison of upper-air (500 hPa level) variables in 20CRv2c with a manual analysis from MeteoSwiss (see also Courvoisier et al., 1979) for 8 August 1978 00:00 UTC (Fig. 6) shows a good spatial agreement of the troughs and ridges, and the temperature distribution: The digging of the trough has further increased at this point in time.

In detail, the 560 gpdm isohypse over Great Britain, France and Germany has a similar shape as the one on the weather maps by Courvoisier et al. (1979). This can be expected, since 20CRv2c is based on (surface) pressure information. Differences appear in the 560 gpdm isohypse reaching further south and the missing 552 gpdm isohypse in 20CRv2c. These effects could stem from either assimilation deficiencies in 20CRv2c or from uncertainties regarding the upper-air soundings or the (manual) interpolation of station information in the weather map.

4.3 Precipitation (dynamics) over the Alps in 20CRv2c

As shown in Figure 3, precipitation amounts on 7 August 1978 differed massively across Switzerland, with extreme values of >300 mm/24 h (>200 mm/24 h) on the south (north) side of the Alps. For comparison, Aebischer (1997) reports a precipitation rate for Zurich of 89 mm/11 h. In 20CRv2c, precipitation rates over the Alps are far lower: Based on 3-hourly precipitation rates, Figure 4 (lower panels) shows extrapolated amounts of 110 mm/24 h along the Alps.

The strong underestimation of precipitation rates is a known deficiency of global reanalyses products (cf. Stucki et al., 2013, for a heavy precipitation event on the south side of the Alps in 1993), where the concave topography of the Alpine bow cannot be resolved. Hence, orographical flow modulations, convergence and lifting of moist air in the concave topography are missed. Instead, rather a deflection of the flow around the smooth 20CRv2c orography is produced in 20CRv2c. This effect may explain why 20CRv2c shows most intense lifting and precipitation values on 7 August 1978 at 12:00 UTC compared to around 18:00 UTC in the reports (*e.g.,* Courvoisier et al., 1979).

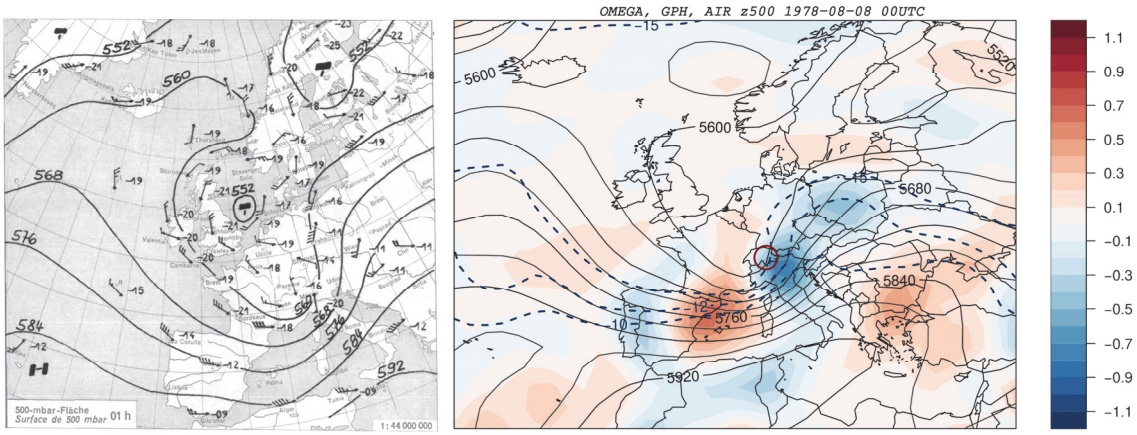

Figure 6. Geopotential height (contours; gpdm), air temperature and wind (vectors, knots) at 500 hPa for 8 August 1978 00:00 UTC, from MeteoSwiss (see also Courvoisier et al. 1979; left panel). Right panel as in Figure 4, but for 8 August 1978 00:00 UTC.

In contrast, 20CRv2c is well capable of depicting important synoptic ingredients for the heavy precipitation in southern and north-eastern Switzerland, *i.e.,* in terms of upper-air circulation and lifting, lower-level advection of moisture and stationarity of the surface front.

An upper-level ingredient is the 'digging' nature of the trough (Lackmann, 2012), which is related to a marked synoptic-scale lifting downwind of the trough axis. Courvoisier et al. (1979) stated that the observed precipitation intensity was only possible with very strong synoptic-scale uplift over Switzerland - 20CRv2c shows the corresponding dynamics.

The presence of deep convection is also indicated by the absence of an elevation gradient in the observed precipitation distribution over Switzerland (Fig. 3), *i.e.,* heavy precipitation was observed at all elevations. Reports of radar signals in Courvoisier et al. (1979) give evidence of increasing thunderstorm activity first in a south-west, north-east band over the Alpine divide, then reaching far into north-eastern Switzerland. The inefficacy of the Alpine barrier in shielding precipitation (no 'Suedstaulage') and the presence of embedded thunderstorms is supported in 20CRv2c by instability and severe-weather measures such as the total totals index.

The track of the surface low around the Alpine bow is similar to the 'Vb-type' described in Courvoisier et al. (1979). Vb cyclones are known to induce heavy precipitation over (the northern side of) the Alps (*e.g.,* Messmer et al., 2015). In addition, the slow propagation of the surface low towards the eastern Alps resembles the quasi-stationary front over the Alps ('STF' type in Stucki et al., 2012) and the NE4 Type 'Amplified trough over the European West Coast' in Giannakaki and Martius (2015), which is conducive to heavy precipitation on both sides of the Alps.

Although the meso-scale dynamics are not shown explicitly in 20CRv2c, wind directions and moisture values in 20CRv2c are supportive to the findings in Courvoisier et al. (1979); in particular that (i) warm-moist air from the south was lifted up the concave, steep southern flanks of the Alps in a confluent and southerly flow, and that (ii) the Alpine valleys north of the divide filled with colder air, resulting in a persistent upgliding process and condensation over the Alps.

5. Summary and conclusion

The flood-inducing heavy precipitation event on 7 August 1978 was characterized by a heterogeneous pattern of precipitation regarding spatial distribution and intensities. It was produced by a massive upglide process of warm-moist air from the south over the Alps and northern Alpine valleys filled with cold air, leading to persistent precipitation and embedded thunderstorms with precipitation amounts reaching up to >300 mm/24 h (>150 mm/24 h) south (north) of the Alps.

In the 20CRv2c dataset, the synoptic-scale ingredients for the heavy precipitation include an approaching mid-tropospheric digging trough with marked vertical lifting downstream, *i.e.,* over the Alps, and advection of very moist, warm air from the south and cooler air from the north. The surface analyses show a 'Vb-type' lee surface low, propagating slowly on the south side of the Alps and leading to a quasi-stationary front associated with heavy precipitation from the afternoon to around midnight on 7 August 1978.

We find that the synoptic-scale atmospheric features are well represented in 20CRv2c, although the coarse grid spacing of 2° x 2° does not allow to capture the meso-scale orographical forcing and modulation of the moisture flow, or the intensity of the local precipitation, for instance. Overall, the performance of 20CRv2c is almost equal to the reanalyses products with 1° x 1° grids, with some reservations regarding details like the intensity of minimum pressure in the lee surface low. Other differences between the analysed four reanalyses products may stem from differing calculations of the variables. We conclude that 20CRv2c is a valid option to analyse extreme events in earlier periods for which no other reanalysis product is available to date.

Acknowledgements

The 20th Century Reanalysis V2c data were provided by the NOAA/OAR/ESRL PSD, Boulder, Colorado, USA, from their Web site at http://www.esrl.noaa.gov/psd/. Support for the Twentieth Century Reanalysis Project dataset is provided by the U.S. Department of Energy, Office of Science Innovative and Novel Computational Impact on Theory and Experiment (DOE INCITE) program, and Office of Biological and Environmental Research (BER), and by the National Oceanic and Atmospheric Administration Climate Program Office. The work was supported by FP7 project ERA-CLIM2, H2020 project EUSTACE, and the Swiss National Science Foundation project EXTRA-LARGE.

References

Aebischer, H. (1997) *Räumlich-zeitliche Analyse der Rhein-Hochwasser.* Diplomarbeit. Geographisches Institut der Univeristät Bern. Bern, Switzerland.

Brönnimann, S. (2017) Weather extremes in an ensemble of historical reanalyses. In: Brönnimann, S. (Ed.) *Historical weather extremes in reanalyses.* Geographica Bernensia G92, p. 7-22, DOI: 10.4480/GB2017.G92.01.

Compo, G. P., J. S. Whitaker, P. D. Sardeshmukh, N. Matsui, R. J. Allan, X. Yin, B. E. Gleason, R. S. Vose, G. Rutledge, P. Bessemoulin, S. Brönnimann, M. Brunet, R. I. Crouthamel, A. N. Grant, P. Y. Groisman, P. D. Jones, M. C. Kruk, A. C. Kruger, G. J. Marshall, M. Maugeri, H. Y. Mok, O. Nordli, T. F. Ross, R. M. Trigo, X. L. Wang, S. D. Woodruff, and S. J. Worley (2011) The Twentieth Century Reanalysis Project. *Q. J. R. Meteorol. Soc.*, **137**, 1–28, doi:10.1002/qj.776.

Conca, A. (1979) L'alluvione del 7/8 agosto 1978. *Wasser, Energie, Luft*, **71**, 202–206.

Courvoisier, H. W., G. A. Gensler, B. Primault, and H. P. Roesli (1979) Das Unwetter vom 7./8. August 1978 in der Schweiz. *Arbeitsberichte der Schweizerischen Meteorol. Anstalt SMA*, 63 pp.

Cram, T. A., G. P. Compo, X. G. Yin, R. J. Allan, C. McColl, R. S. Vose, J. S. Whitaker, N. Matsui, L. Ashcroft, R. Auchmann, P. Bessemoulin, T. Brandsma, P. Brohan, M. Brunet, J. Comeaux, R. Crouthamel, B. E. Gleason, P. Y. Groisman, H. Hersbach, P. D. Jones, T. Jonsson, S. Jourdain, G. Kelly, K. R. Knapp, A. Kruger, H. Kubota G. Lentini, A. Lorrey, N. Lott, S. J. Lubker, J. Luterbacher, G. J. Marshall, M. Maugeri, C. J. Mock, H. Y. Mok, O. Nordli, M. J. Rodwell, T. F. Ross, D. Schuster, L. Srnec, M. A. Valente, Z. Vizi, X. L. Wang, N. Westcott, J. S. Woollen, and S. J. Worley (2015) The International Surface Pressure Databank version 2. *Geosci. Data J.*, **2**, 31–46, doi:10.1002/gdj3.25.

Doswell, C. A., H. E. Brooks, and R. A. Maddox (1996) Flash Flood Forecasting: An Ingredients-Based Methodology. *Weather Forecast.*, **11**, 560–581, doi:10.1175/1520-0434(1996)011<0560:FFFAIB>2.0.CO;2.

FOEN (2017) Swiss Federal Office for the Environment FOEN - Hydrological data and forecasts for Maggia - Locarno, Solduno (EDV: 2368), retrieved online at http://www.hydrodaten.admin.ch/en/2368.html

Frei, C. and C. Schaer (1998) A precipitation climatology of the Alps from high-resolution rain-gauge observations. *Int. J. Climatol.*, **18**, 873–900.

Froidevaux, P. and O. Martius (2013) Exceptional moisture transport towards orography : a precursor to severe floods in Switzerland. **13**, 1–13, doi:10.1002/qj.2793.

Giannakaki, P. and O. Martius (2015) Synoptic-scale flow structures associated with extreme precipitation events in northern Switzerland. *Int. J. Climatol.*, **2515**, 2497–2515, doi:10.1002/joc.4508.

Hauenstein, W. (2009) Wasserkraft und Klimawandel. *Wasser, Energie Luft*, **101**, 127–132.

Heitmann, A. and G. Zanetti (1979) *L'alluvione : immagini e testimonianze del 7/8 agosto 1978 nella svizzera italiana*. Tipografia. G. Zanetti, Ed. Tipografia Stazione, Dadò, Locarno, 131 pp.

Kalnay, E., M. Kanamitsu, R. Kistler, W. Collins, D. Deaven, L. Gandin, M. Iredell, S. Saha, G. White, J. Woollen, Y. Zhu, M. Chelliah, W. Ebisuzaki, W. Higgins, J. Janowiak, K. C. Mo, C. Ropelewski, J. Wang, A. Leetmaa, R. Reynolds, R. Jenne, and D. Joseph (1996) The NCEP/NCAR 40-year reanalysis project. **77**, 437–471, doi:10.1175/1520-0477(1996)0772.0.CO;2.

Lackmann, G. (2012) *Midlatitude synoptic meteorology : dynamics, analysis, and forecasting*. American Meteorological Society, Boston, MA, 388 pp.

Laloyaux, P., M. Balmaseda, D. Dee, K. Mogensen, and P. Janssen (2016) A coupled data assimilation system for climate reanalysis. *Q. J. R. Meteorol. Soc.*, **142**, 65–78, doi:10.1002/qj.2629.

Messmer, M., J. J. Gómez-Navarro, and C. C. Raible (2015) Climatology of Vb cyclones, physical mechanisms and their impact on extreme precipitation over Central Europe. *Earth Syst. Dyn.*, **6**, 541–553, doi:10.5194/esd-6-541-2015.

Piaget, N., P. Froidevaux, P. Giannakaki, F. Gierth, O. Martius, M. Riemer, G. Wolf, and C. M. Grams (2015) Dynamics of a local Alpine flooding event in October 2011: Moisture source and large-scale circulation. *Q. J. R. Meteorol. Soc.*, **141**, 1922–1937, doi:10.1002/qj.2496.

Poli, P., H. Hersbach, D. P. Dee, P. Berrisford, A. J. Simmons, F. Vitart, P. Laloyaux, D. G. H. Tan, C. Peubey, J. N. Thepaut, Y. Tremolet, E. V. Holm, M. Bonavita, L. Isaksen, and M. Fisher (2016) ERA-20C: An atmospheric reanalysis of the twentieth century. *J. Clim.*, **29**, 4083–4097, doi:10.1175/JCLI-D-15-0556.1.

Röthlisberger, G. (1991) *Chronik der Unwetterschäden in der Schweiz*. Eidgenössische Forschungsanstalt für Wald Schnee und Landschaft Birmensdorf, Birmensdorf, 122 pp.

Scherrer, S., A. Petrascheck, and H. Hodel (2006) Extreme Hochwasser des Rheins bei Basel – Herleitung von Szenarien. *Wasser Energie Luft*, **98**, 42–48.

Stucki, P., R. Rickli, S. Brönnimann, O. Martius, H. Wanner, D. Grebner, and J. Luterbacher (2012) Weather patterns and hydro-climatological precursors of extreme floods in Switzerland since 1868. *Meteorol. Zeitschrift*, **21**, 531–550, doi:10.1127/0941-2948/2012/368.

Stucki, P., O. Martius, S. Brönnimann, and J. Franke (2013) The extreme flood event of Lago Maggiore in September 1993. In: Brönnimann S., and O. Martius (Eds.) *Weather extremes during the past 140 years*, 53–58, doi:10.4480/GB2013.G89.06.

van Bebber, W. J. (1891) Die Zugstrassen der barometrischen Minima nach Bahnenkarten der Deutschen Seewarte für den Zeitraum von 1870–1890. *Meteorol. Zeitschrift*, **8**, 361–366.

VAW (1979) *Jahresbericht 1978*. Versuchsanstalt für Wasserbau, Hydrologie und Glaziologie der ETH Zürich VAW, Zürich, 106 pp.